JOURNAL OF THE ROYAL SOCIETY INTERFACE

Mechanics and optimization of undulatory locomotion in different environments, tuning geometry, stiffness, damping and frictional anisotropy

Journal:	*Journal of the Royal Society Interface*
Manuscript ID	rsif-2022-0875.R1
Article Type:	Research
Date Submitted by the Author:	10-Jan-2023
Complete List of Authors:	Yaqoob, Basit; University of Trento, Department of Civil, Environmental and Mechanical Engineering; Istituto Italiano di Tecnologia, Laboratory of Bioinspired Soft Robotics, Center for Convergent Technologies Rodella, Andrea; University of Rome La Sapienza, Department of Structural and Geotechnical Engineering Del Dottore, Emanuela; Istituto Italiano di Tecnologia, Laboratory of Bioinspired Soft Robotics, Center for Convergent Technologies Mondini, Alessio; Istituto Italiano di Tecnologia, Laboratory of Bioinspired Soft Robotics, Center for Convergent Technologies Mazzolai, Barbara; Istituto Italiano di Tecnologia, Laboratory of Bioinspired Soft Robotics, Center for Convergent Technologies Pugno, Nicola; University of Trento, Department of Civil, Environmental and Mechanical Engineering; Queen Mary University of London, School of Engineering and Materials Science
Categories:	Life Sciences - Engineering interface
Subject:	Biomathematics < CROSS-DISCIPLINARY SCIENCES, Biomechanics < CROSS-DISCIPLINARY SCIENCES, Biomimetics < CROSS-DISCIPLINARY SCIENCES
Keywords:	Undulatory Locomotion, Limbless Animal Locomotion, Optimization, Mechanics, Serpentine Locomotion, Biomechanics

Author-supplied statements

Relevant information will appear here if provided.

Ethics

Does your article include research that required ethical approval or permits?:
This article does not present research with ethical considerations

Statement (if applicable):
CUST_IF_YES_ETHICS :No data available.

Data

It is a condition of publication that data, code and materials supporting your paper are made publicly available. Does your paper present new data?:
My paper has no data

Statement (if applicable):
CUST_IF_YES_DATA :No data available.

Conflict of interest

I/We declare we have no competing interests

Statement (if applicable):
CUST_STATE_CONFLICT :No data available.

Mechanics and optimization of undulatory locomotion in different environments, tuning geometry, stiffness, damping and frictional anisotropy

Basit Yaqoob[1, 2] Andrea Rodella[3], Emanuela Del Dottore[2], Alessio Mondini[2], Barbara Mazzolai[2], and Nicola M. Pugno [*1,4]

[1]*Laboratory for Bioinspired, Bionic, Nano, Meta Materials and Mechanics, Department of Civil, Environmental and Mechanical Engineering, University of Trento, Trento, Italy.*

[2]*Laboratory of Bioinspired Soft Robotics, Center for Convergent Technologies, Istituto Italiano di Tecnologia, Genova, Italy.*

[3]*Department of Structural and Geotechnical Engineering, Sapienza University of Rome, Italy*

[4]*School of Engineering and Materials Science, Queen Mary University of London, London, UK.*

*Corresponding Author: nicola.pugno@unitn.it

Abstract

One of the oldest yet most common modalities of locomotion known among limbless animals is undulatory, also recognized for its stability compared to legged locomotion. Multiple forms of active, e.g., active gait control, and passive mechanisms, e.g., body morphology and material properties, have adapted to different environments. The current research explores the passive role of body stiffness and internal losses in meeting terrain requirements. Furthermore, it addresses the influence of the environment on the resultant gait and how the interplay between various environments and body properties can lead to different speeds. We modeled undulatory locomotion in a dry-friction environment where frictional anisotropy determines propulsion. We found that the body stiffness, the moment of inertia, the dry frictional coefficient ratio between normal and tangential frictional constants, and the internal damping of the body play an essential role in optimizing speed and animal adaptability to external conditions. Furthermore, we demonstrate that various known gaits like swimming, crawling, and polychaete-like locomotion are achieved as a result of the interaction between body and environment parameters. Moreover, we validated the model by retrieving a corn snake's speed using data from the literature. This study demonstrates that the dependence between morphology, body material properties, and environment can be exploited to design long-segmented robots to perform in specialized situations.

Keywords

Biomechanics, Undulatory locomotion, Optimization based on physical properties

Introduction

In nature, locomotion is an inherent necessity of some living organisms to forage for food, escape danger, or mate. Undulatory locomotion is widespread among typically legless, long-thin-bodied organisms, as it is the optimal solution for these living beings [1]. Exhibition of this movement is found in aquatic and terrestrial animals. Furthermore, subarenaceous animals like sandfish exploit the aptness of lateral undulations for moving in sub-surfaces without using their limbs [2].

The lateral travel of sinusoidal waves along the length of a body characterizes undulatory locomotion. J. Gray first formulated that, in undulatory locomotion, a body interacts with the environment so that the force of propulsion is generated due to frictional anisotropy (direction-dependent friction) [3,4]. However, several other factors synergistically play an important role in generating efficient undulatory locomotion in adaptation to environmental constraints.

From a morphological perspective, it is supported by experiments that scales on the ventral side of the body assist in generating a frictional anisotropy [5–7]. Besides providing traction, scales also enhance control and help in maneuverability by allowing the animals to lift their bodies. The animal can control each scale with a muscle [8,9] and enhance maneuverability by controlling contact points and frictional anisotropy. Results drawn by comparing the performance of a shovel-nosed snake and a sandfish lizard show that long cylindrical bodies also favour undulatory locomotion [10]. In addition, sandfish experiments have shown that the head shape is responsible for lift and drag forces required for better maneuverability during their underground undulatory locomotion [11]. A tapered head produces 18% less drag and 20% higher speed than a uniform body [12].

Furthermore, limbless animals can also enhance their performance by modulating different gaits. For example, among sidewinding Figure 1(a) and lateral undulation Figure 1(b), lateral undulation is hypothesized to be more energy efficient at higher speeds, whereas sidewinding at moderate speeds [13]. Moreover, the cost per cycle of sidewinding is lower than concertina Figure 1(d) and lateral undulatory locomotion, as investigated by [14]. Undulatory locomotion can further be categorized into swimming and crawling-like modes, Figure 1(e, f). Here, we define swimming-like locomotion where amplitude along the body length increases from head to tail. In contrast, in crawling-like locomotion, the amplitude decreases from head to tail Figure 1(e, f) for any environment without discriminating by the number of contact points. Note that the contact points are where friction is active and do not necessarily present in each link, as we are assuming here for simplicity. In swimming-like locomotion, the speed of the organism is observed to be faster than in crawling [15]. Another kind of undulatory locomotion in some organisms is polychaete-like, in which the direction of the traveling wave is the same as the displacement direction. The difference between lateral undulatory and polychaete-like locomotion is illustrated in Figure 1(b, c). In polychaete-like locomotion, organisms are not totally limbless but have special attachments along their body length called parapodia, Figure 2 (a), and because of their interaction with the environment, these attachments might have a crucial role in defining locomotion [16].

Both active and passive mechanisms have evolved to act effectively in a specific environment and adapt to changes in environmental properties. In the case of fluidic environments, a change in the fluid viscosity triggers a switch between swimming and crawling-like behaviors. When viscosity increases, the undulation wavelength and frequency in *C. elegans* decrease [17] with the increase of the drag force [18,19]. The impact of a change in environment on the resultant gait is also shown in [20] using mathematical modeling. A factor in changing the body waveform from swimming to crawling is a muscle activity change, as observed in *C. elegans* [21] and lungfish [22,23]. For lungfish, at higher velocities [22] and also at higher viscous environments [24], more muscles are recruited to produce thrust. In *C. elegans* the propagation of ventral muscle activity towards the posterior is observed to be faster in swimming than in crawling [21]. Besides neural control, factors like changes in body properties and environment are also involved in the transition from swimming to crawling [25,26]. In dry environments, snakes can modulate swimming-like, and crawling-like locomotion by passive mechanics adapting to frictional forces exercised on the body. In a high frictional environment, crawling-like behavior is the dominant mode in snakes, Figure 2(b), while they move with swimming-like behavior on smooth substrates, Figure 2(c). Physical constraints provided by the environment also affect motion performance. A. Parashar *et. al.* validated this hypothesis by making worms move in waved channels of varying amplitudes [27]. It was observed that worms moved faster and more steadily when the channel matched the natural body-wave characteristics.

As discussed above, physical factors are involved in optimizing the performance of undulatory locomotion. To attain terrain adaptability and energy compensation, it is crucial to change the way of exploiting the interaction between the body and the substrate [5–9], modulating various gaits [13,14], and having efficient physical features [10]. There are some studies for the mathematical quantification of these physical parameters using computational fluid dynamics (CFD) [29] and non-linear resistive penalty models [30]. These studies revealed that the stiffness of the body could be used to optimize undulatory kinematics. To our knowledge, the mathematical quantification of different physical performance parameters like frictional anisotropy, stiffness, internal losses, and moment of inertia in a combined form is not yet studied. Here, we model the undulatory locomotion and relate different design and tribological parameters to optimize and quantify motion. We will look at the interconnection between the moment of inertia, joint stiffness, internal damping, and frictional anisotropy expressed as the ratio between normal and tangential frictional coefficients, and we will show different modes of locomotion induced by the interplay between these physical quantities. Many organisms show passive dynamics, as observed in snakes when facing unplanned collisions [31]. We also investigate 'morphological intelligence', defined as the use of passive properties of the body to perform various tasks [32]. The current study explores this morphological intelligence by analyzing the relative contribution of listed physical properties in showcasing different undulatory locomotion gaits. The proposed model is validated using experimental data of a corn snake reported in [5,8].

Mathematical Modeling

A modular body of a limbless animal is assumed to be composed of "N" finite number of links, joined together by "N-1" visco-elastic springs, as shown in Figure 3. The damping factor of a rotational dashpot is represented by b_i, and the stiffness constant of a rotational spring is denoted by k_i. Here, i designates the joint number between the "i-th" and "$i+1$-th" link. We assume that each spring and dashpot have the same spring constant (k) and damping factor (b), respectively. The length of the link is represented by l_i while "l_{tot}" is the total length of system. Here, we are assuming that the total length is divided into equal-length segments such that $l_i = l_{tot}/N$, $i \in [1,N]$. u_x and u_y are x and y coordinates of the starting points of the first link with respect to a global coordinate system. $s_i \in [0,l_i]$ represents points along the length of the i-th link, and θ_i is the link angle which is measured anticlockwise.

Frictional forces are generated along normal and tangential directions (as shown in Figure 3) because of the orthotropic friction between links and ground. The force of friction is opposite to the direction of velocity and is given by equations *(1)* and *(2)*:

$$\vec{T}_i = -g\mu_t m_i \, sgn(v_{t,i})\hat{t}_i \qquad (1)$$

$$\vec{N}_i = -g\mu_n m_i \, sgn(v_{n,i})\hat{n}_i \qquad (2)$$

Here $i \in [1,N]$, and g is the gravitational acceleration, μ_t and μ_n are dry frictional constants along tangential and normal directions, respectively, Figure 3 , m_i is the mass of i-th link, which we are considering the same for every link so $m_i = m$, and sgn is the sign function. $\hat{t}_i$ and $\hat{n}_i$ are unit vectors in the tangential and normal directions (see Supplementary Information) which translate forces of friction to a local coordinate system. Tangential and normal velocities are given by $\vec{v}_{t,i} = \dot{\vec{r}}_i.\hat{t}_i$ and $\vec{v}_{n,i} = \dot{\vec{r}}_i.\hat{n}_i$, respectively, where $\vec{r}_i$ is the position vector, and the dot represents the time derivative. We replaced sgn function according to the equation *(3)* for the sake of continuity in the numerical model:

$$\mathrm{sgn}(f(x)) \simeq \left[\frac{f(x)}{\sqrt{f(x)^2+\varepsilon}}\right] \qquad (3)$$

Here, the smaller the value of ε, the more accurate the approximation would be. Euler-Lagrange equation of the motions can be obtained following the lagrangian approach, accordingly *(4)*:

$$\frac{d}{dt}\left(\frac{\partial L}{\partial \dot{q}_h}\right) - \frac{\partial L}{\partial q_h} = Q_{h,Dry} - \frac{\partial R}{\partial \dot{q}_h} \qquad (4)$$

where q_h is the set of the unknown generalized coordinate system, L is the Lagrangian of the system, $Q_{h,Dry}$ represents losses because of friction, and R represents energy loss because of internal damping [33]. Further description of the model is provided in Supplementary Information.

Non-Dimensionalization

The non-dimensional form is achieved through following substitutions $u_x = l_{tot}\tilde{u}_x$, $u_y = l_{tot}\tilde{u}_y$, $\mathrm{t} = \tau\tilde{t}$, $\mu = \mu_n/\mu_t$, $s_i = l_i\tilde{s}_i$, $\tilde{u}_x$ and $\tilde{u}_y$ are dimensionless x and y coordinates of the starting point of the links system. τ is the period of oscillations, and $\tilde{t}$ is the dimensionless time. $\tilde{s}_i$ is a dimensionless number that indicates the dimensionless length of the i-th link such that $\tilde{s}_i \in [0,1]$. Replacing dimensional quantities with their non-dimensional equivalents, as defined above, produces:

$$\frac{d}{d\tilde{t}}\left(\frac{\partial \tilde{\mathrm{L}}}{\partial \tilde{\dot{q}}_h}\right) + \frac{\partial \tilde{\mathrm{L}}}{\partial \tilde{q}_h} - \alpha_{\mathrm{Dry}}\tilde{Q}_{h,Dry} + \beta\frac{\partial \tilde{R}}{\partial \tilde{\dot{q}}_h} = 0 \qquad (5)$$

Here $\tilde{L}$ is the Lagrangian function in the non-dimensionalized form defined by *(6)*, $\tilde{Q}_{h,Dry}$ is the dimensionless dissipation due to friction, and $\tilde{R}$ is the dimensionless internal viscous losses. α_{Dry} and β are dimensionless quantities directly related to the normal frictional constant and internal damping, respectively, and are defined by *(7)* and *(8)*:

$$\tilde{L}\left(\tilde{\dot{\mathrm{q}}}_{\mathrm{h}},\tilde{\mathrm{q}}_{\mathrm{h}},\tilde{\mathrm{t}}\right) = \sum_{i=1}^{N} \dot{\tilde{\vec{r}}}_{i,1/2}^{T} \cdot \dot{\tilde{\vec{r}}}_{i,1/2} + \mathrm{A}\sum_{i=1}^{N} \tilde{\dot{\theta}}_i^2 - \mathrm{B}\sum_{i=1}^{N-1} (\theta_{i+1} - \theta_i)^2 \qquad (6)$$

$$\alpha_{\mathrm{Dry}} = \frac{2g\tau^2\mu_n}{l_{tot}} \qquad (7)$$

$$\beta = \mathrm{N}\frac{b\tau}{m_{tot}l_{tot}^2} \qquad (8)$$

In equation *(6)*, $\dot{\tilde{\vec{r}}}_{i,1/2}$ is the dimensionless position vector of the center point of i-th link ($\tilde{s}_i = 1/2$). constants A and B are directly related to the moment of inertia and joint stiffness, respectively, and are defined according to *(9)* and *(10)*:

$$\mathrm{A} = N\frac{I}{m_{tot}l_{tot}^2} \qquad (9)$$

$$\mathrm{B} = N\frac{\tau^2 k}{m_{tot} l_{tot}^2} \qquad (10)$$

Here, *I* is the moment of inertia considered the same for every link, and m_{tot} is the total mass, such that $m_i = m_{tot}/N$ is the mass of the i-th link. Harmonic excitation in the system is introduced by soliciting the end link angle sinusoidally, as given by equation *(11)*:

$$\theta_N(\tilde{t}) = \mathrm{asin}\,[2\pi\tilde{t}] \qquad (11)$$

Where a is the angular amplitude (see Supplementary Information for further details).

The total energy ($\tilde{E}_{tot}$) of the system is evaluated as the sum of the energy dissipated by viscous forces $(\tilde{E}_{out})$ and work done by constraint forces $(\tilde{E}_{in})$. See Supplementary Information for detailed definitions.

Validation Settings

We selected corn snakes as our test organism and utilized data retrieved from the literature to validate the model. When snakes move, it is known that they do not have the entire body in contact with the ground [5]. The concertina is the most complex within lateral undulatory locomotions, requiring the highest number of contact points. Nevertheless, H. Marvi *et al.* noticed that snakes make less than seven contact points during concertina locomotion in open spaces and utilized three links in their theoretical modeling [9]. By convention, for lateral undulatory locomotion, three contact points are considered [3,34,35]. In our model, every link is in contact with the ground; consequently, for the validation test, we discretized the snake body into three links to follow the convention, and we considered the geometry of a thin rod. To visualize a more realistic motion, in all other simulations, we used a higher number of links (N=5) (the Results section also reports an analysis of the effects of the number of links). The mass and length of the corn snake are used as reported in [8] (mass=0.73 [kg], length=1.313 [m]). We used the torsional stiffness of the scale of a corn snake to be $k_i = 0.01196\ [Nm]$ as calculated by H. Marvi. et al. [8]. Normal frictional coefficient (μ_n) is taken as 0.2, as experimentally observed for corn snakes in an unconscious state [5]. We set the angular amplitude of undulation (a) as $7\pi/37\ [rad]$, which is in the range as specified in [5], and the frequency is fixed at 1.5 [Hz] [36]. We estimated the damping and tangential coefficient of friction with a snake velocity of 2.7 [cm/s] [5], and then results are compared with the biological model.

Results

For the validation of the model, experimental data is substituted to find out the optimum value of the internal damping constant (*b*) and tangential frictional coefficient (μ_t) corresponding to the speed of 0.027 [m/s] [5], which are found to be 0.15±0.025 [Nms/rad] and 0.05±0.01, respectively, Figure 4. We noticed that our estimated dry frictional coefficient ratio is 4 at 0.027 [m/s], which is in the same order of magnitude as the experimental value equal to 1.82 [5].

We then characterized undulatory locomotion using dimensionless constants based on environment and body properties. Normal frictional coefficient, internal damping, moment of inertia, stiffness, and the ratio between normal and tangential friction components are directly correlated with constants α_{Dry}, β, A, B, and μ, respectively. Using these constants, we can characterize and optimize various modes of undulatory locomotion.

Figure 5(a) shows the interdependence between stiffness (B) and internal damping (β) factors to achieve the desired speed. Here, we can optimize speed based on stiffness and internal damping factors by fixing the remaining factors. Optimal values of stiffness and internal damping are given in Figure 5 (a) in a scenario providing a dry frictional coefficient ratio of μ = 50. In this scenario, the maximum speed is reached with a stiffness factor B = 175 and an internal damping β = 10.4. In the same scene, by setting the optimal B and β found, we can explore the inertial factor (A) and dry frictional factor (α_{Dry}) domain and find the combination providing the maximum displacement, as observed in Figure 5(b). From Figure 5, we concluded that undulatory locomotion speed strongly depends on frictional, internal damping, inertial, and stiffness factors. This interdependence can be exploited in physical situations to achieve the desired speed. For example, the deployment of a robot in a specific environment can be made more efficient based on its stiffness and geometry optimization. The dry frictional coefficient ratio (μ) and dry frictional factor (α_{Dry}) characterize the environment-body interaction in our formalized constants. Deciding factors of the environment affecting ground-body interaction include surface roughness, texture, and material properties. This information can be used to design features and ventral asperities of the body to reach the desired performance in a specific environment. Similarly, based on the properties of the body, the definition of an ideal environment is also possible, where the body can reach its maximum performance. In this case, the performance can be tuned by acting on the characteristics of the environment, if possible.

Further characterization of the motion revealed the transition from crawling-like to swimming-like behavior. We noticed that crawling-like locomotion is triggered when the dry frictional factor is greater than the stiffness factor Figure 6(a). While with swimming-like locomotion, the stiffness factor is greater than the dry frictional factor Figure 6(b). Animations of these behaviors are provided in supplementary videos 1 and 2.

Looking at the energy and the speed, they are directly proportional to each other Figure 7(a, b). Stiffness, inertial, and internal damping factors depend on the number of links except for the dry frictional factor, equations *(7)*, *(8)*, *(9)*, and *(10)*. Increasing links increases stiffness members in the system; consequently, the system's stiffness factor and potential energy increase. Likewise, the internal damping factor, on increasing links, increases internal damping points in the system; hence, internal losses also increase. However, the dry frictional factor and the dry frictional coefficient ratio remained the same, but increasing links also increased contact points which have an overall increasing effect on frictional losses ($Q_{h,Dry}$). That is why it is observed that higher number of links perform better in low frictional environment: it is required a higher number of contact points to provide propulsion, Figure 7(a). On the contrary, a system with fewer contact points, thus fewer links, requires higher frictional anisotropy. This phenomenon is also reported in [13], where it was found that the lateral undulatory gait with less number of contact points required higher frictional anisotropy to perform better. Hence, an increasing number of links by keeping the dry frictional factor constant increases speed until the domination of frictional and internal losses because of the rise in contact points and internal damping factors, respectively, Figure 7(b). In addition, the inertial factor is also inversely proportional to the number of links keeping total mass and length constant (see Supplementary Information).

When the dry frictional coefficient ratio (μ) is reduced to less than 1, polychaete-like locomotion is observed, Figure 1(c). On the other hand, when the dry frictional coefficient ratio is greater than 1, the direction of the traveling body wave is opposite to the direction of motion, leading to lateral undulatory locomotion, Figure 1(b). Results showed that polychaete-like locomotion could also be optimized based on frictional, stiffness, internal damping, and inertial factors, see Figure 8(a, b). The comparison of the influence of the dry frictional coefficient ratio on lateral undulatory and polychaete-like locomotion showed opposite results. In the case of undulatory locomotion, increasing the dry frictional coefficient ratio increases the displacement. Eventually, it reaches the saturation point

where further increases do not have much effect, Figure 8(c). Whereas, in the case of polychaete-like locomotion, motion can be optimized based on the dry frictional coefficient ratio, Figure 8(d).

Discussion

We proposed a non-dimensional model to analyze the role of physical quantities, such as stiffness, moment of inertia, frictional anisotropy, and internal damping in undulatory locomotion. We found that the desired locomotion is achieved with proper tuning of these physical quantities. Furthermore, we observed that the optimum set of derived constants at maximum displacement has a greater stiffness factor than the dry frictional factor, Figure 5(a, b). When the body stiffness increases, the energy storage capacity increases, which enhances the elastic potential energy of the body to overcome frictional energy losses. In this scenario, we observed that body wave amplitude increases from anterior to posterior, as shown in Figure 6(b) (Supplementary Video1), gaining a swimming-like behavior. When dissipation forces are dominant, body wave amplitude decreases from anterior to posterior, Figure 6(a) (Supplementary Video 2), leading to crawling-like behavior. The speed in the former case is higher than in the latter. The pattern of increasing amplitude from anterior to posterior is observed among organisms swimming in water or on land [21,37]. Muscles in living beings serve the purpose of energy storage elements like springs [38]. It has been observed that increasing muscle engagement increases speed, which means muscle activity increases, and more muscles get recruited to achieve high speed [22,24]. For example, a study on the activity of two different kinds of muscles, called red and white, in eels showed that only red muscles are used at slower speeds. In comparison, at higher speeds, white muscles are additionally recruited. In addition, the stiffness role has also been tested in *C. elegans*, and it has been observed that mutants with deteriorated muscles and cuticles moved slower [39]. Frictional anisotropy cannot be neglected in undulatory locomotion. In fact, it is predominantly a friction-based motion where frictional forces overcome inertial forces [19,40,41]. The challenge of adapting to different terrains can be addressed better if the effects of stiffness and friction are synergized together, which is supported by studies on animals. For example, in nematodes, when their environment changes, they shift between different modes of locomotion and speed. During swimming in the water, the body's waveform characteristics differ significantly from crawling on harder media, like agar, in terms of amplitude, wavelength, and speed [17,21,42,43]. Recently, the influence of the shape and orientation of scales have been explored for lateral undulatory locomotion [44–46]. However, according to the authors' knowledge, the characterization of body frictional and stiffness properties has never been done before. We hypothesized that the passive adaptability of the body according to the dynamic scenarios can be exploited for energy efficiency, simplicity, and weight reduction. Indeed, these qualities are desirable for micro-robots (e.g., that are needed to release in the human body) or in situations where onboard electronic components should be avoided, for example, when operating in a high-radiation environment or when recovery of the device is not feasible.

Polychaete-like locomotion, in which body waves travel in the same direction as the direction of movement, is achieved by setting a dry frictional coefficient ratio smaller than one. In reality, polychaetes have numerous parapodia along their body (Figure 2(a)), making tangential frictional coefficient larger than normal frictional coefficient [16]. Previously, it has also been realized in robots by setting normal frictional constant less than the tangential coefficient [47,48]. We observed that it is not an efficient mode of locomotion compared to normal undulatory locomotion. Simulations suggest the significance of parapodia in animals for polychaete-like locomotion. Without parapodia, locomotion is slow and does not closely mimic natural movements; however, we can successfully initiate polychaete-like locomotion by setting the appropriate dry frictional coefficient ratio and can investigate the role of passive properties of the environment and the body (Supplementary Video 3).

In the validation part, the tangential frictional and damping constants are varied, as shown in Figure 4. We found that values of μ_t = 0.05±0.01 and b = 0.15±0.025 [Nms/rad] , correspond to the snake speed of 2.7 [cm/s] as mentioned in [5]. Our theoretically estimated dry frictional coefficient ratio (μ) is 4, higher than the coefficient ratio of 1.82 recoded from milk-snake [5]. This discrepancy could be due to the model simplification that cannot capture the real model complexity at this stage. In fact, it has been observed that snakes lift their bodies during locomotion in such a way that only the points of zero curvature are in contact with the ground [5]. In this way, it has been observed that their efficiency increases. However, in our modeling, we compromise the body's shape continuity by using three links to compensate for comparable contact points. In addition, mechanical properties differ along the length of snake bodies [49,50], and their body's cross-section area and mass distribution also change. Also, partially the reported frictional constants could be underestimated because it has been observed that the frictional constant of a conscious snake is higher than in an unconscious one. During locomotion, snakes can change the orientation of their scales as muscles control scales, while in their unconscious state, it is impossible [51]. Furthermore, they can increase the force on contact points with the ground during the movement by increasing the push provided by muscles. By these considerations, our estimation might be more realistic than the value found experimentally.

Conclusions

The effects of physical quantities, such as stiffness, moment of inertia, frictional anisotropy, and internal damping, are studied here for undulatory locomotion. It has been established that the exploitation of body and environment features in situated physical systems can promote the passive locomotion of the body into its environment, gaining advantages in terms of energy consumption, adaptability, lightweight, and minimal use of electronic components. It is hypothesized that properties of the body can be optimized to get desired speed depending upon the environment, which can assist in developing soft specialized segmented robots in the deemed surrounding, and vice versa. The proposed theoretical model successfully captured different modes of locomotion, like swimming, crawling, and polychaete-like movements. It is found that during crawling, dissipation dominates stiffness, while in swimming, stiffness dominates dissipation. Despite model simplifications, feeding our model with experimental data has produced results in good agreement with the experimentally calculated dry frictional coefficient ratio of a corn snake, considering an underestimation due to the unconsciousness of the snake in the experimental tests. This study can be applied to developing better adaptable bio-inspired robots for search and rescue, exploration, and medical applications. Further validation of this hypothesis on a physical system is our future goal.

Author Contributions:

BM, AR, NMP conceived and NMP, BM, AR, EDD, AM supervised the study. BY designed the methodology, analyzed the data, and prepared the original manuscript. AM, EDD, AR helped in reviewing and editing the final manuscript.

Funding Statement

NMP is supported by the Italian Ministry of Education MIUR, Italy under the PRIN-20177TTP3S.

References

1. Hicks G, Ito K. 2005 A method for determination of optimal gaits with application to a snake-like serial-link structure. *IEEE Trans. Automat. Contr.* **50**, 1291–1306. (doi:10.1109/TAC.2005.854583)

2. Maladen RD, Ding Y, Li C, Goldman DI. 2009 Undulatory Swimming in Sand: Subsurface

Locomotion of the Sandfish Lizard. *Science (80-.).* **325**, 314–318. (doi:10.1126/science.1172490)

3. Gray J. 1946 The mechanism of locomotion in snakes. *J. Exp. Biol.* **23**, 101–120.
4. Gray J. 1951 Undulatory propulsion in small organisms. *Nature* **168**, 929–930. (doi:10.1038/168929a0)
5. Hu DL, Nirody J, Scott T, Shelley MJ. 2009 The mechanics of slithering locomotion. *Proc. Natl. Acad. Sci.* **106**, 10081–10085. (doi:10.1073/pnas.0812533106)
6. Abdel-Aal HA. 2018 Review of Friction and Surface Properties of Snakeskin. In *Journal of the Mechanical Behavior of Biomedical Materials*, pp. 276–315. (doi:10.4018/978-1-5225-2993-4.ch012)
7. Abdel-Aal HA. 2018 Surface structure and tribology of legless squamate reptiles. *J. Mech. Behav. Biomed. Mater.* **79**, 354–398. (doi:10.1016/j.jmbbm.2017.11.008)
8. Marvi H, Cook JP, Streator JL, Hu DL. 2016 Snakes move their scales to increase friction. *Biotribology* **5**, 52–60. (doi:10.1016/j.biotri.2015.11.001)
9. Marvi H, Hu DL. 2012 Friction enhancement in concertina locomotion of snakes. *J. R. Soc. Interface* **9**, 3067–3080. (doi:10.1098/rsif.2012.0132)
10. Sharpe SS, Koehler SA, Kuckuk RM, Serrano M, Vela PA, Mendelson J, Goldman DI. 2014 Locomotor benefits of being a slender and slick sand-swimmer. *J. Exp. Biol.* **218**, 1111–1111. (doi:10.1242/jeb.108357)
11. Maladen RD, Umbanhowar PB, Ding Y, Masse A, Goldman DI. 2011 Granular lift forces predict vertical motion of a sand-swimming robot. In *2011 IEEE International Conference on Robotics and Automation*, pp. 1398–1403. IEEE. (doi:10.1109/ICRA.2011.5980301)
12. Ding Y, Sharpe SS, Masse A, Goldman DI. 2012 Mechanics of Undulatory Swimming in a Frictional Fluid. *PLoS Comput. Biol.* **8**, 354–398. (doi:10.1371/journal.pcbi.1002810)
13. Ariizumi R, Matsuno F. 2017 Dynamic Analysis of Three Snake Robot Gaits. *IEEE Trans. Robot.* **33**, 1075–1087. (doi:10.1109/TRO.2017.2704581)
14. SECOR SM, JAYNE BC, BENNETT AF. 1992 LOCOMOTOR PERFORMANCE AND ENERGETIC COST OF SIDEWINDING BY THE SNAKE CROTALUS CERASTES. *J. Exp. Biol.* **163**, 1–14. (doi:10.1242/jeb.163.1.1)
15. G J, Lissmann HW. 1964 the Locomotion of Nematodes. *J. Exp. Biol.* **41**, 135–154.
16. Spina G La, Sfakiotakis M, Tsakiris DP, Menciassi A, Dario P. 2007 Polychaete-Like Undulatory Robotic Locomotion in Unstructured Substrates. *IEEE Trans. Robot.* **23**, 1200–1212. (doi:10.1109/TRO.2007.909791)
17. Fang-Yen C, Wyart M, Xie J, Kawai R, Kodger T, Chen S, Wen Q, Samuel ADT. 2010 Biomechanical analysis of gait adaptation in the nematode Caenorhabditis elegans. *Proc. Natl. Acad. Sci.* **107**, 20323–20328. (doi:10.1073/pnas.1003016107)
18. Backholm M, Kasper AKS, Schulman RD, Ryu WS, Dalnoki-Veress K. 2015 The effects of viscosity on the undulatory swimming dynamics of C. elegans. *Phys. Fluids* **27**, 091901. (doi:10.1063/1.4931795)
19. Sznitman J, Shen X, Purohit PK, Arratia PE. 2010 The Effects of Fluid Viscosity on the Kinematics and Material Properties of C. elegans Swimming at Low Reynolds Number. *Exp.*

Mech. **50**, 1303–1311. (doi:10.1007/s11340-010-9339-1)

20. Guo Z V., Mahadevan L. 2008 Limbless undulatory propulsion on land. *Proc. Natl. Acad. Sci. U. S. A.* **105**, 3179–3184. (doi:10.1073/pnas.0705442105)
21. Pierce-Shimomura JT, Chen BL, Mun JJ, Ho R, Sarkis R, McIntire SL. 2008 Genetic analysis of crawling and swimming locomotory patterns in C. elegans. *Proc. Natl. Acad. Sci.* **105**, 20982–20987. (doi:10.1073/pnas.0810359105)
22. Gillis GB. 1998 Neuromuscular control of anguilliform locomotion: patterns of red and white muscle activity during swimming in the american eel anguilla rostrata. *J. Exp. Biol.* **201**, 3245–3256. (doi:10.1242/jeb.201.23.3245)
23. Biewener AA, Gillis GB. 1999 Dynamics of muscle function during locomotion: accommodating variable conditions. *J. Exp. Biol.* **202**, 3387–3396. (doi:10.1242/jeb.202.23.3387)
24. Horner AM, Jayne BC. 2008 The effects of viscosity on the axial motor pattern and kinematics of the African lungfish (Protopterus annectens) during lateral undulatory swimming. *J. Exp. Biol.* **211**, 1612–1622. (doi:10.1242/jeb.013029)
25. Boyle JH, Berri S, Cohen N. 2012 Gait Modulation in C. elegans: An Integrated Neuromechanical Model. *Front. Comput. Neurosci.* **6**, 1–15. (doi:10.3389/fncom.2012.00010)
26. Berri S, Boyle JH, Tassieri M, Hope IA, Cohen N. 2009 Forward locomotion of the nematode C. elegans is achieved through modulation of a single gait. *HFSP J.* **3**, 186–193. (doi:10.2976/1.3082260)
27. Parashar A, Lycke R, Carr JA, Pandey S. 2011 Amplitude-modulated sinusoidal microchannels for observing adaptability in C. elegans locomotion. *Biomicrofluidics* **5**, 024112. (doi:10.1063/1.3604391)
28. Semenov A. 2017 Alitta Virens Swimming. See https://flic.kr/p/V2L1UN.
29. Tytell ED, Leftwich MC, Hsu C-Y, Griffith BE, Cohen AH, Smits AJ, Hamlet C, Fauci LJ. 2016 Role of body stiffness in undulatory swimming: Insights from robotic and computational models. *Phys. Rev. Fluids* **1**, 073202. (doi:10.1103/PhysRevFluids.1.073202)
30. Bhalla APS, Griffith BE, Patankar NA. 2013 A Forced Damped Oscillation Framework for Undulatory Swimming Provides New Insights into How Propulsion Arises in Active and Passive Swimming. *PLoS Comput. Biol.* **9**, e1003097. (doi:10.1371/journal.pcbi.1003097)
31. Schiebel PE, Rieser JM, Hubbard AM, Chen L, Rocklin DZ, Goldman DI. 2019 Mechanical diffraction reveals the role of passive dynamics in a slithering snake. *Proc. Natl. Acad. Sci.* **116**, 4798–4803. (doi:10.1073/pnas.1808675116)
32. Sitti M. 2021 Physical intelligence as a new paradigm. *Extrem. Mech. Lett.* **46**, 101340. (doi:10.1016/j.eml.2021.101340)
33. Rodella A. 2020 Analytical and Numerical Modelling of Undulatory Locomotion for Limbless Organisms in Granular/Viscous Media. University of Trento. (doi:10.15168/11572_273235)
34. Gasc JP, Cattaert D, Chasserat C, Clarac F. 1989 Propulsive action of a snake pushing against a single site: Its combined analysis. *J. Morphol.* **201**, 315–329. (doi:10.1002/jmor.1052010310)
35. Sarrafan S, Malayjerdi M, Behboudi M, Akbarzadeh A. 2013 Determination of optimum number of ground contact points in modeling a snake-like robot with maneuverability in three dimensions. In *2013 First RSI/ISM International Conference on Robotics and*

Mechatronics (ICRoM), pp. 158–164. IEEE. (doi:10.1109/ICRoM.2013.6510098)

36. Jayne BC. 1986 Kinematics of Terrestrial Snake Locomotion. *Copeia* **1986**, 915. (doi:10.2307/1445288)

37. Gillis GB. 1998 Environmental effects on undulatory locomotion in the American eel Anguilla rostrata: kinematics in water and on land. *J. Exp. Biol.* **201**, 949–961. (doi:10.1242/jeb.201.7.949)

38. Dickinson MH, Farley CT, Full RJ, Koehl MAR, Kram R, Lehman S. 2000 How Animals Move: An Integrative View. *Science (80-.).* **288**, 100–106. (doi:10.1126/science.288.5463.100)

39. Karbowski J, Cronin CJ, Seah A, Mendel JE, Cleary D, Sternberg PW. 2006 Conservation rules, their breakdown, and optimality in Caenorhabditis sinusoidal locomotion. *J. Theor. Biol.* **242**, 652–669. (doi:10.1016/j.jtbi.2006.04.012)

40. McHenry MJ, Azizi E, Strother JA. 2003 The hydrodynamics of locomotion at intermediate Reynolds numbers:undulatory swimming in ascidian larvae (Botrylloides sp.). *J. Exp. Biol.* **206**, 327–343. (doi:10.1242/jeb.00069)

41. Cohen N, Boyle JH. 2010 Swimming at low Reynolds number: a beginners guide to undulatory locomotion. *Contemp. Phys.* **51**, 103–123. (doi:10.1080/00107510903268381)

42. Park S, Hwang H, Nam S-W, Martinez F, Austin RH, Ryu WS. 2008 Enhanced Caenorhabditis elegans Locomotion in a Structured Microfluidic Environment. *PLoS One* **3**, e2550. (doi:10.1371/journal.pone.0002550)

43. Mesce. 2010 Shared strategies for behavioral switching: understanding how locomotor patterns are turned on and off. *Front. Behav. Neurosci.* **4**, 354–398. (doi:10.3389/fnbeh.2010.00049)

44. Shen D, Zhang Q, Wang C, Wang X, Tian M. 2021 Design and Analysis of a Snake-Inspired Crawling Robot Driven by Alterable Angle Scales. *IEEE Robot. Autom. Lett.* **6**, 3744–3751. (doi:10.1109/LRA.2021.3061379)

45. Serrano MM, Chang AH, Guangcong Zhang, Vela PA. 2015 Incorporating frictional anisotropy in the design of a robotic snake through the exploitation of scales. In *2015 IEEE International Conference on Robotics and Automation (ICRA)*, pp. 3729–3734. IEEE. (doi:10.1109/ICRA.2015.7139717)

46. Branyan C, Hatton RL, Menguc Y. 2020 Snake-Inspired Kirigami Skin for Lateral Undulation of a Soft Snake Robot. *IEEE Robot. Autom. Lett.* **5**, 1728–1733. (doi:10.1109/LRA.2020.2969949)

47. Sfakiotakis M, Tsakiris DP. 2007 Biomimetic Centering for Undulatory Robots. *Int. J. Rob. Res.* **26**, 1267–1282. (doi:10.1177/0278364907083394)

48. Tsakiris D, Menciassi A, Sfakiotakis M, La Spina G, Dario P. 2004 Undulatory locomotion of polychaete annelids: mechanics, neural control and robotic prototypes. *Annu. Comput. Neurosci. Meet.*

49. Rivera G, Savitzky AH, Hinkley JA. 2005 Mechanical properties of the integument of the common gartersnake, Thamnophis sirtalis (Serpentes: Colubridae). *J. Exp. Biol.* **208**, 2913–2922. (doi:10.1242/jeb.01715)

50. Jayne BC. 1988 Mechanical behaviour of snake skin. *J. Zool.* **214**, 125–140. (doi:10.1111/j.1469-7998.1988.tb04991.x)

51. Marvi H, Meyers G, Russell G, Hu DL. 2011 Scalybot: A Snake-Inspired Robot With Active

Control of Friction. In *ASME 2011 Dynamic Systems and Control Conference and Bath/ASME Symposium on Fluid Power and Motion Control, Volume 2*, pp. 443–450. ASMEDC. (doi:10.1115/DSCC2011-6174)

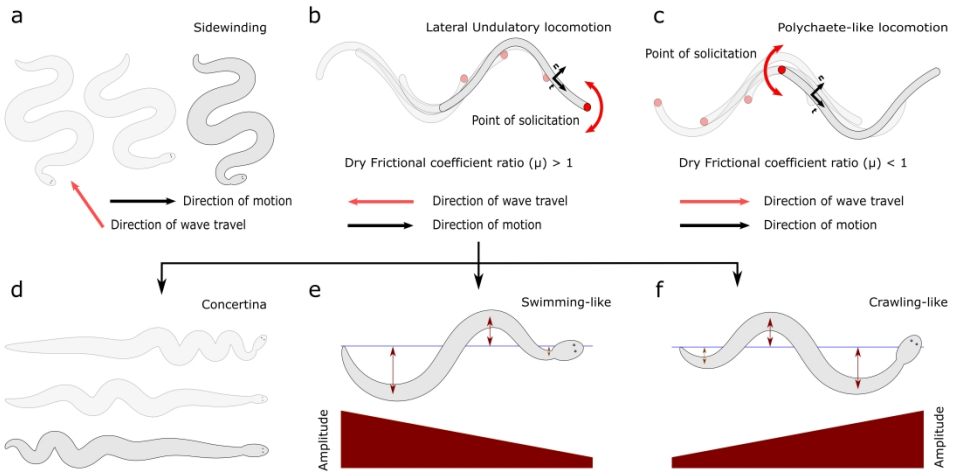

Figure 1: Different modes of undulatory locomotion as observed in snakes (a, b, d, f) and generally long cylindrical limbless animals (b, c, e, f). (a) In sidewinding, static contact points with the ground result in disconnected tracks oblique to the direction of motion. (b) In lateral undulatory locomotion, the direction of the traveling wave is opposite to the direction of motion, and the dry frictional coefficient ratio ($\mu = \mu_n/\mu_t$) between normal (n) and tangential (t) direction is greater than 1. We have divided the undulatory locomotion further into concertina (d), swimming-like (e), and crawling-like (f) motion. (c) In polychaete-like locomotion, the direction of the traveling body wave is along the same direction of motion, and the dry frictional coefficient ratio is less than 1. (d) Concertina locomotion. Half of the body has lateral bendings in this mode, and the other half makes a rectilinear motion. Forward motion is achieved by the sequential transfer of these two modes along the body length. This mode of locomotion is observed in narrow tunnels with insufficient space for lateral bending. (e) In swimming, the amplitude is shown to be increasing from anterior to posterior. (f) In crawling, the amplitude is shown to be decreasing from anterior to posterior.

1325x655mm (115 x 115 DPI)

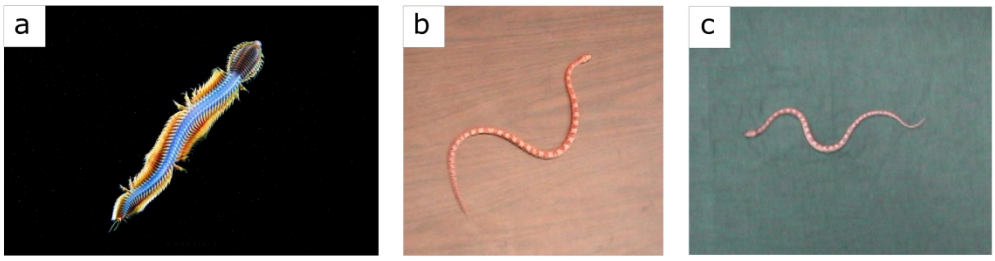

Figure 2: (a) Polychaete-like locomotion exhibited by Alitta virens. Photo courtesy of Alexander Semenov [28]. (b) Swimming-like locomotion of a corn snake (Pantherophis guttatus) on plastic. Picture by courtesy of David hu, Georgia Tech. (c) Crawling-like locomotion of a corn snake on cloth. Picture by courtesy of David hu, Georgia Tech.

420x114mm (181 x 181 DPI)

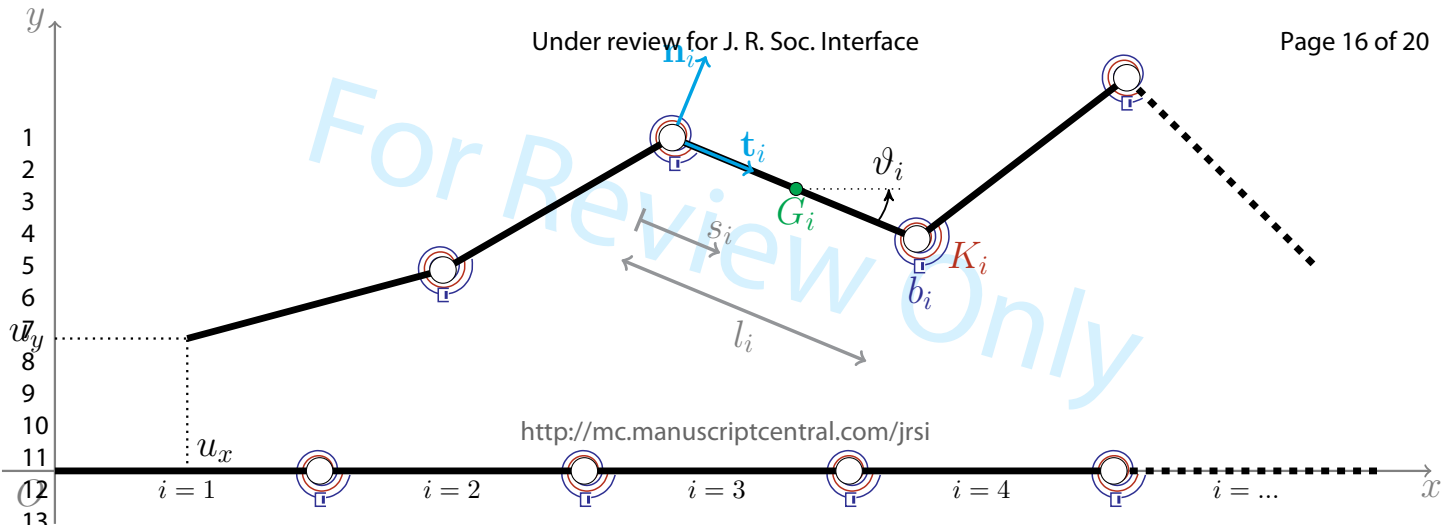

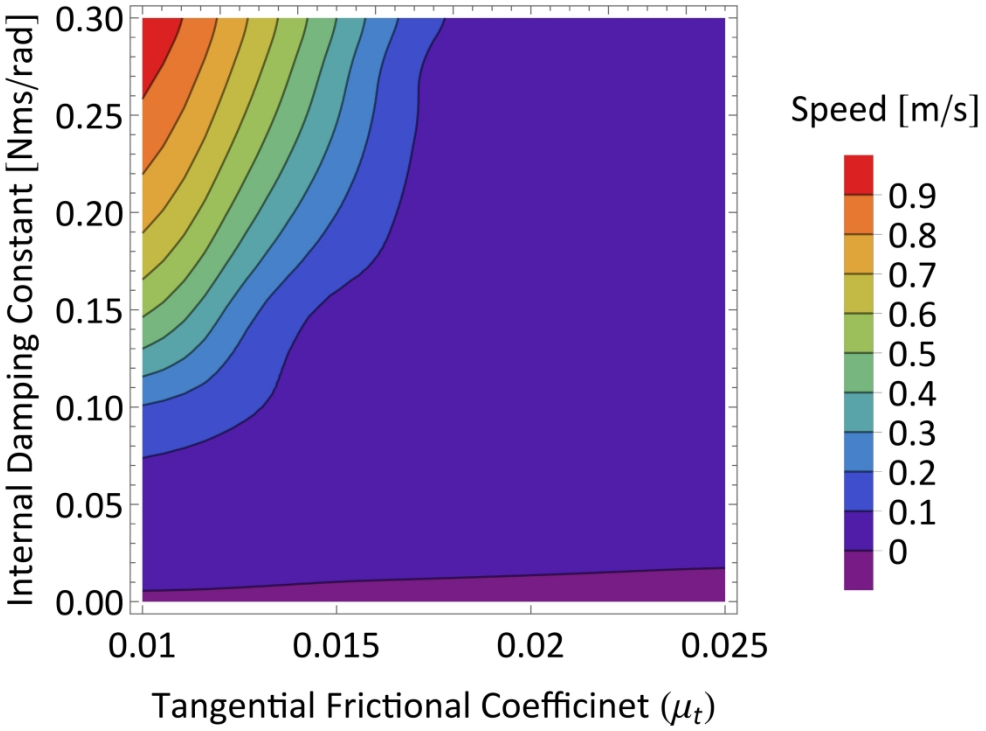

Figure 4: Damping and tangential frictional constants are varied with intervals of 0.025 [Nms/rad] and 0.01, respectively. A solution corresponding to the average velocity of 0.027 [m/s] is selected.

164x120mm (600 x 600 DPI)

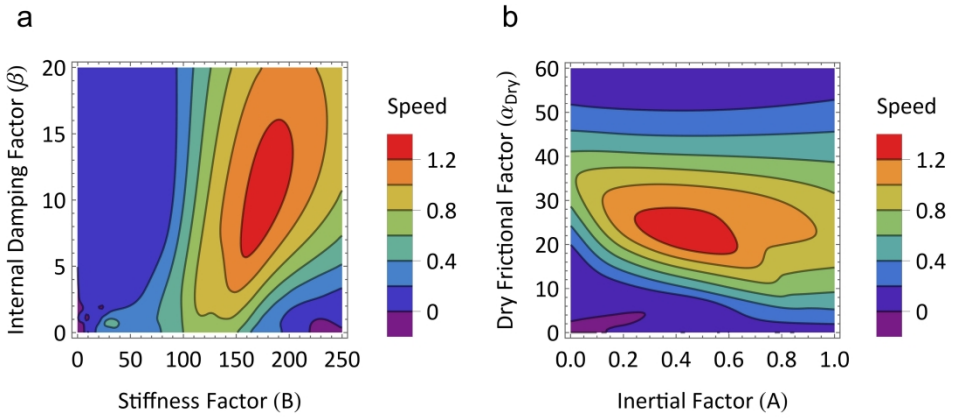

Figure 5: The interdependence of stiffness, internal damping, and inertial and dry frictional factors needed to achieve a desired dimensionless speed for lateral undulatory locomotion. Simulations are run at an angular amplitude of a=8π/125 [rad], dry frictional coefficient ratio μ =50, and the number of links N=5. The speed shown is the dimensionless speed of the system's center of mass. The multiplicative factor to convert dimensionless speed into dimensional form is l_{tot}/\tau. (a) This figure shows speed optimization based on stiffness and internal damping factors. The maximum speed value is achieved at 175±5 and 10.4±0.8 values of B and β, respectively. Inertial and dry frictional factors are kept constant at 0.5 and 20, respectively (b) Speed optimization is achieved from inertial and dry frictional factors. Obtained optimum values of inertial and dry frictional factors are 0.46±0.02 and 22±1, respectively. Stiffness and internal damping factors are kept constant at 175 and 10.4, respectively.

176x88mm (600 x 600 DPI)

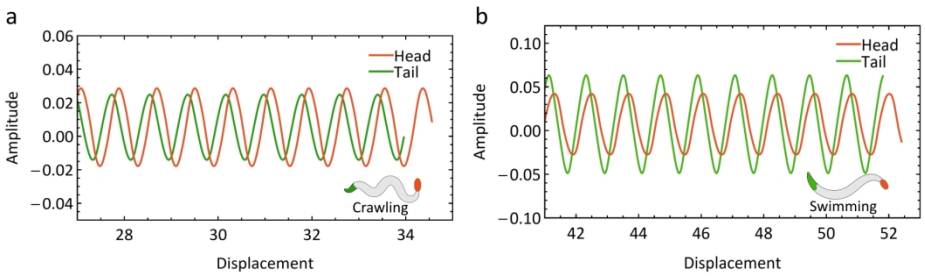

Figure 6: Simulations are run at angular amplitude = 8π/125 [rad], damping factor = 1, Inertial factor = 0.5, number of links N=5, and dry frictional coefficient ratio = 50. The multiplicative factor to convert dimensionless displacement and amplitude into dimensional form is l_{tot} (a) In crawling-like locomotion, it can be observed that the amplitude of a head is larger than a tail. The dry frictional factor is 50, and the stiffness factor is 40, i.e., α_{Dry}>B. (b) depiction of swimming-like locomotion, the amplitude of the head is smaller than the tail. The stiffness factor is set at 175 and the dry frictional factor at 40, i.e., B>α_{Dry}.

564x173mm (90 x 90 DPI)

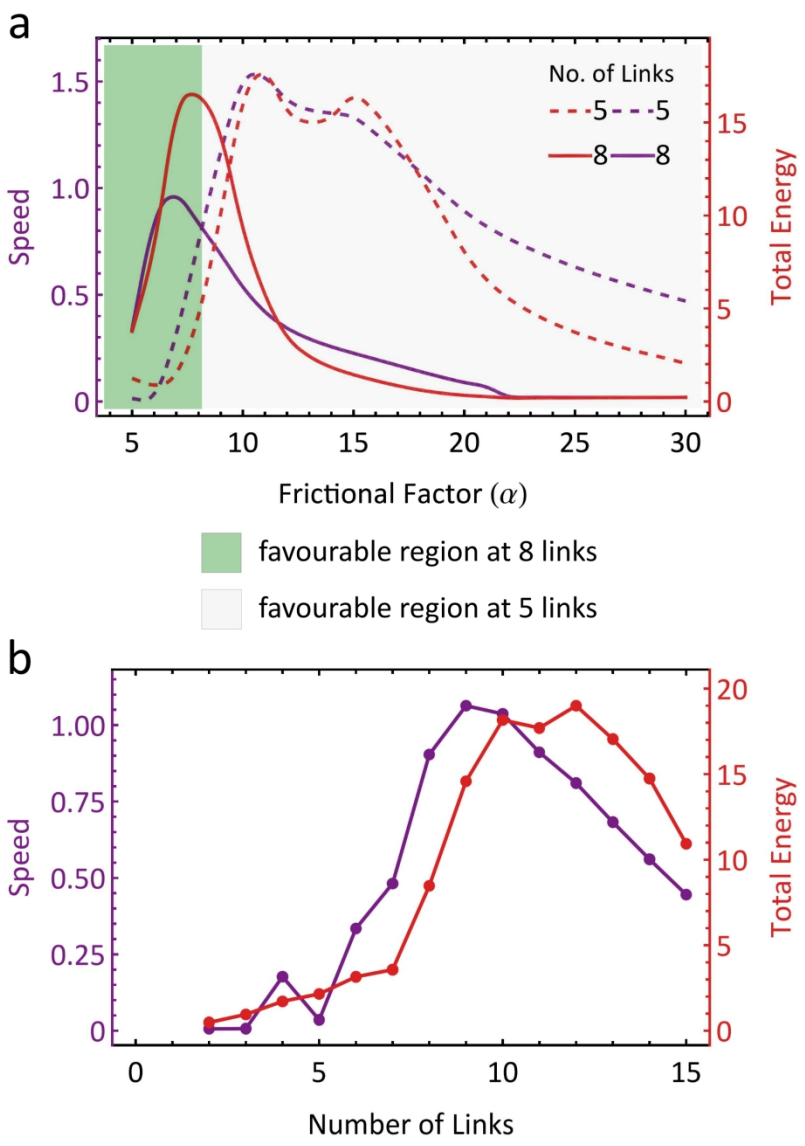

Figure 7: Effect of the number of links and the trend of energy. Simulations are run as A=0.25/N^2, B=5N, β=N/5, a=8π/125 [rad], and μ=50. The multiplicative factor to convert dimensionless total energy into respective dimensions is \frac{2N\tau^2}{m_{tot}l_{tot}^2}. (a) It shows the impact of an increasing number of links on speed and energy in relation to the dry frictional factor. More links are shown to be advantageous in a low-frictional anisotropic environment. Contrarily, fewer links perform better in a high-frictional environment. (b) When all factors are kept constant, as stated earlier, and the dry frictional factor is kept constant at 5, we can observe the optimum number of links in that environment.

267x381mm (190 x 190 DPI)

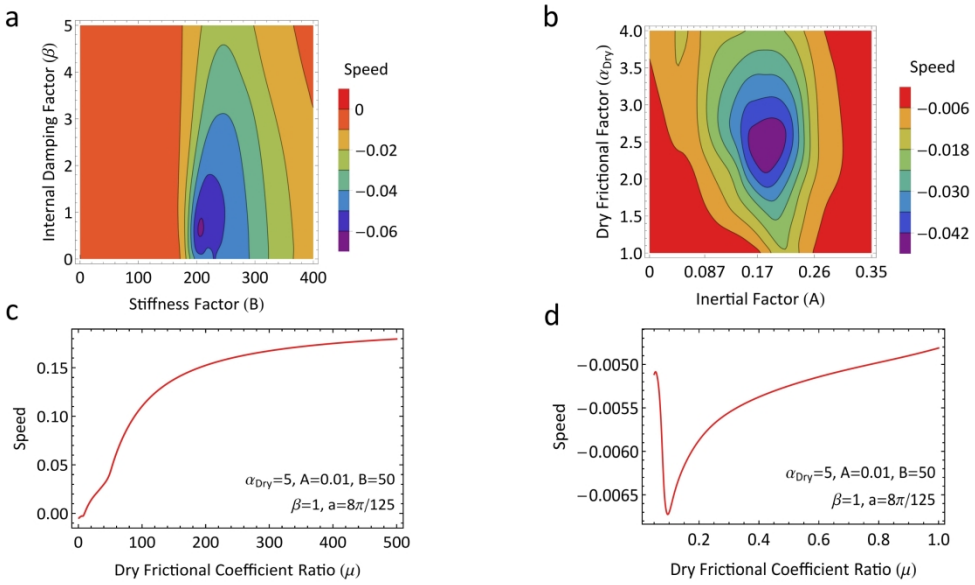

Figure 8: (a, b) Optimization of polychaete-like locomotion based on stiffness and internal damping factors. Simulation is run at angular amplitude (a) = 8π/125 [rad], Inertial Factor (A) = 0.5, dry frictional coefficient ratio (μ) = 0.01, dry frictional factor (α_{Dry}) = 5, and number of links (N=5). (a) Maximum value of dimensionless speed is achieved at internal damping factor (β) = 0.6±0.2 and stiffness factor (B) = 208±8. (b) Optimization of polychaete-like locomotion based on inertial and dry frictional factors, which come out to be 0.196±0.014 and 1.32±0.12, respectively. Where stiffness factor (B) =100, dry frictional coefficient ratio (μ) = 0.01, damping factor (β) = 0.6, angular amplitude (a) = 8π/125 [rad]. (c) The trend of dimensionless speed with increasing value of the dry frictional coefficient ratio in the case of lateral undulatory locomotion. (d) Relationship between dimensionless speed and dry frictional coefficient ratio in the case of polychaete-like locomotion.

504x296mm (151 x 151 DPI)